

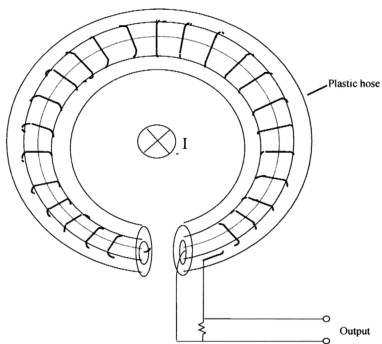
## CHAPTER 3

### DIAGNOSTICS AND INSTRUMENTATION

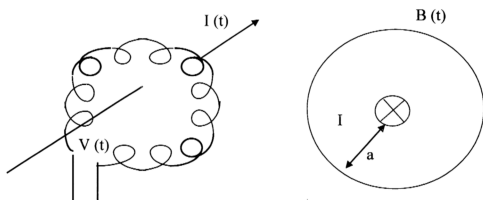
The diagnostics and instrumentation used in the experiments involve the measurements of  $dI/dt$ , the electron beams and X-rays. The current produced by the discharge of the system is measured by a Rogowski coil. Electron beams are detected by a charge collector. PIN diode is used to record the temporal evolution of the intensity of X-rays emitted from electron beam target interaction. The energy of the electron beam can be deduced from the PIN diode signals by using the foil absorption technique. By using these diagnostics, the energy and the temporal evolution of the electron beam in the THCD are investigated.

#### 3.1 The Rogowski Coil

A Rogowski coil is essentially a multi-turn wire wound on a polythene tube and then bent into the shape of a torus. The wire is returned through the end turn of the coil back to the initial end to minimize the effect of flux threading the major opening of the torus, as shown in Figure 3.1(a). In the ideal situation, the current to be



(a)



(b)

Figure 3.1 The Rogowski coil.

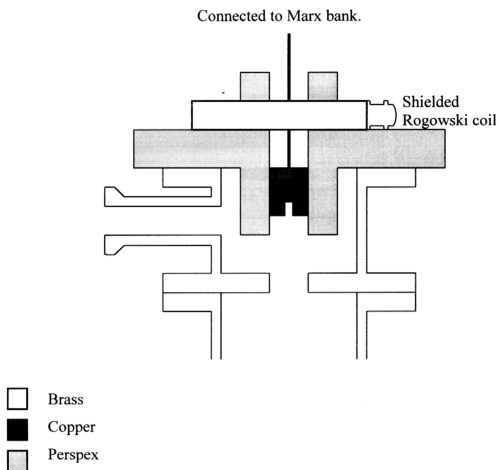


Figure 3.2 The schematic diagram showing the mounting of the Rogowski coil

measured  $I(t)$  is expected to pass through the centre of the major cross-section of the torus, as shown in Figure 3.1(b). Then by using Ampere's law, the magnetic field induced by the current at the axis of the minor cross-section of the torus is given by

$$B(t) = \left( \frac{\mu_0 I(t)}{2\pi a} \right) \quad (3.1)$$

where  $a$  is the major radius of the torus and  $\mu_0 = 4\pi \times 10^{-7} \text{ Hm}^{-1}$  is the permeability of vacuum.

If the minor cross-sectional area of the torus is  $A$ , then the magnetic flux that threads the minor cross-section of the torus is

$$\Phi(t) = \left( \frac{\mu_0 A}{2\pi a} \right) I(t) \quad (3.2)$$

Thus the voltage induced across the terminals of the coil is

$$V(t) = \left( \frac{\mu_0 A n}{2\pi a} \right) \frac{dI}{dt} \quad (3.3)$$

where  $n$  is the number of turns of the coil. From equation (3.3), the induced voltage is proportional to the rate of change of the current ( $dI/dt$ ) and not the current itself. By integrating the voltage with respect to time, the current,  $I$ , can be obtained.

The position where the Rogowski coil is mounted onto the THCD system is shown in Figure 3.2. The Rogowski coil consists of 120 turns of enameled copper wire. It is concealed inside a Brass shield and placed on the hollow cathode holder.

### 3.2 Charge Collector

The simplest form of charged particle detector is a charge collector to collect the charges deposited in it. In this project, the charge collector is made from a copper disc with a cross sectional area of  $4.4 \times 10^{-2} \text{ m}^2$ . The thickness of the disc should be as thin as possible to increase the sensitivity of the charge collector. The disc is connected via a copper wire to a BNC free plug. The charge collector is biased at +45 V. This biasing voltage is to enhance the collection of the electrons and to repel the ions which are ejected by the electron beam from the copper disc surface. The set-up of the charge collector is shown in Figure 3.3 and the biasing circuit of the charge collector is shown in Figure 3.4.

In order to minimize the pickup of noises, secondary electrons and X-rays, a shield, made from a cylindrical plastic hose which is wrapped by copper foil, is used to cover the charge collector. The copper foil is extended towards the open end of the hose and leaves a hole of about 8 mm diameter. The hole allows electrons to pass through and deposit on the disc. A bigger hole will allow more electrons to be collected but it may also introduce more noise to the signal. The disc is about 85 mm below the hollow cathode. A brass disc, which has a BNC plug mounted at the centre of the disc, is used to mount the charge collector onto the target chamber.

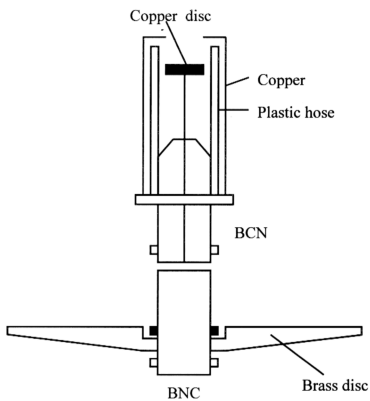


Figure 3.3 The setup shows the charge collector with the copper disc connects directly to the BNC plug.

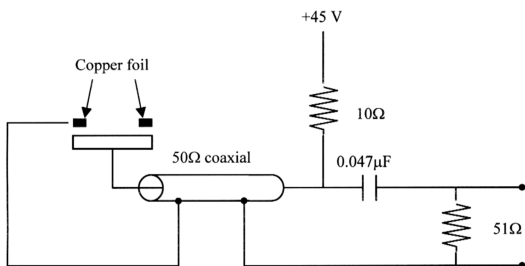


Figure 3.4 Biasing circuit for the charge collector.

### 3.3 PIN Diodes As X-Ray Detectors

Silicon PIN diodes are convenient x-ray detectors for X-ray measurement of the Transient Hollow Cathode Discharge. Their simple construction, fast response and high sensitivity allow them to be widely used for x-ray detection. Actually, a PIN diode consists of a thin disc of silicon, which is an intrinsic layer, sandwiched between a layer of p-type and a layer of n-type Si semiconductor. The front surface, where the x-ray enter, is the n-layer and is often called ‘dead layer’. It is maintained at ground potential. The rear p-layer is biased at a negative potential using the circuit shown in Figure 3.5.

The X-ray PIN diodes used in this work are BPX-65 and Quantrad model 100-PIN-250 with the following specifications:

a) for BPX-65 model:

Effective detection area	1 mm <sup>2</sup>
Intrinsic Si wafer thickness	10 μm
Dead layer thickness	0.5 μm
Rise time (typical)	0.5 ns

b) for Quantrad 100 PIN-250 model:

Effective detection area	100 mm <sup>2</sup>
Intrinsic Si wafer thickness	250 μm
Dead layer thickness	0.80 μm
Rise time (typical)	2 ns



The BPX-65 PIN diode is placed inside a TO-18 casing with a glass window. The glass window has been removed for the purpose of X-ray detection. The diode is biased at -45 V ( circuit shown in Figure 3.5 ). The 100 – PIN - 250 model is biased at -300V with a similar circuit.

The sensitivity  $S(\lambda)$  of the PIN diode can be expressed as ( *D. M. Corallo et. al., 1980*) :

$$S(\lambda) = 0.282\exp(-\mu x_n)[1 - \exp(-\mu x_i)] \quad A\,W^{-1}, \tag{3.4}$$

where  $\mu$  is the mass-absorption coefficient of silicon which is a function of x-ray photon energy  $h\nu$ ;  $x_n$  and  $x_i$  are the mass thickness of the dead layer and the intrinsic layer respectively. The calculated sensitivity curve of the Quantrad 100-PIN-250 diode is shown in Figure 3.6. The singularity at 6.7Å is due to the K-absorption edge of silicon.

### 3.4 Calculation Of Mass-Absorption Coefficient ( $\mu$ )

Numerous calculation on the mass absorption coefficient  $\mu$  have been made by a number of workers semi-empirically [*J. A. Victoreen, 1949*], [*V. F. Aleksin et. al.,1966*], [*E. P. Bertin, 1970*]. However, their calculation of mass absorption coefficient is unable to cover a sufficient wide range of wavelengths.

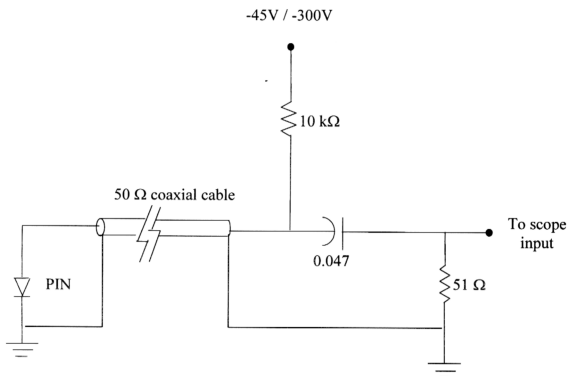


Figure 3.5 Biasing circuit of the PIN-diode.

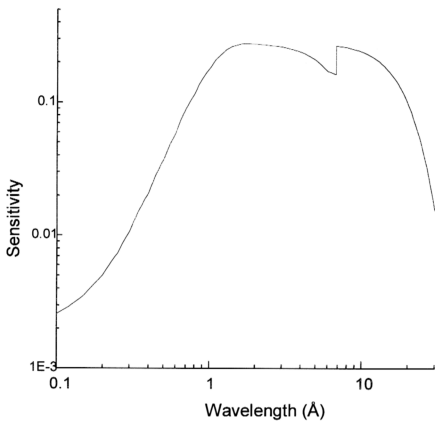


Figure 3.6 The sensitivity curve of the 100-PIN-250 diode.

An expression that is generally valid for all elements at wavelength shorter than the K-absorption edge is given by [J. A. Victoreen, 1943]:

$$\mu(\lambda) = C\lambda^3 - D\lambda^4 + \sigma_e N_A \left( \frac{Z}{A} \right) \text{ cm}^2\text{g}^{-1} , \quad (3.5)$$

where  $\lambda$  is the wavelength in Å;  $N_A$  is the Avogadro's number,  $6.02 \times 10^{23} \text{ gmol}^{-1}$ ;  $\sigma_e$  is the scattering coefficient for each electron and is given by Klein Nishina formula [O. Klein and Y. Nishina, 1928];

$$\sigma_e = \pi l_0^2 \left[ \frac{2 + 2\alpha_0}{\alpha_0^2} \left( \frac{2[1 + \alpha_0]}{1 + 2\alpha_0} - \frac{1}{\alpha_0} \log[1 + 2\alpha_0] \right) + \frac{1}{\alpha_0} \log[1 + 2\alpha_0] - 2 \frac{1 + 3\alpha_0}{(1 + 2\alpha_0)^2} \right] , \quad (3.6)$$

with  $l_0 = e^2/mc^2 = 2.8197 \times 10^{-13} \text{ cm}$  (the classical electron radius);

$$\alpha_0 = h\nu/mc^2;$$

$e$  is the electronic charge,  $4.803 \times 10^{-10} \text{ e.s.u.}$ ;

$m$  is the electron mass,  $9.11 \times 10^{-28} \text{ g}$ ;

$h$  is the Planck constant,  $6.626 \times 10^{-27} \text{ ergs}$ ;

$c$  is the speed of light,  $2.998 \times 10^{10} \text{ cms}^{-1}$ ;

$$\nu = c/\lambda;$$

$C, D$  are constants for a particular elements and were tabulated by J. A. Victoreen [J. A. Victoreen, 1949]; and  $Z, A$  are the atomic number and atomic weight (in gram) of the element respectively.

The values of C, D, Z, Z/A as well as the wavelength of K-absorption edge of several elements of interests in the present study are listed in Table 3.1[J. A. Victoreen, 1949].

Elements	Z	Z/A	C (cm <sup>2</sup> g <sup>-1</sup> Å <sup>-1</sup> )	D (cm <sup>3</sup> g <sup>-1</sup> Å <sup>-1</sup> )	λ <sub>K</sub> (Å) *	λ <sub>L</sub> (Å)
H	1	0.9922	0.01274	4.66 X 10 <sup>-6</sup>		
C	6	0.5000	1.224	0.0142	43.68	
O	8	0.5000	3.178	0.0654	23.32	
Al	13	0.482	14.6	0.8362	7.94813	
Si	14	0.4989	18.47	1.144	6.738	
Cu	29	0.4561	178.5	51.73	1.38059	13.288

\* [J. Beardeen, 1967]

Table 3.1

For wavelengths between the K-absorption edge and L-absorption edge, an expression for element with Z < 20 is given by [V. F. Aleksin et. al.,1966]:

$$\mu(\lambda) = 5.153 \times 10^{-4} \frac{Z^{4.3}}{\lambda} \lambda^3 \qquad \text{cm}^2\text{g}^{-1}$$

The value of  $\mu(\lambda)$  calculated from this expression is 2 times higher than the values determined experimentally [E.P Bertin, 1970], hence a factor of  $\frac{1}{2}$  has to be included when using this expression.

A common X-ray absorber used in the present study is the aluminized mylar which is mylar coated with very thin aluminium ( $\sim 1000 \text{ \AA}$ ). The aluminium coating is used to cut off the visible light because mylar is a transparent substance. The thickness of the aluminium is negligible when compared to the mylar. Hence, only the mass-absorption coefficient  $\mu_{\text{mylar}}$  for the mylar is considered. Since mylar is a composite substance (with chemical formula  $\text{C}_{10}\text{H}_8\text{O}_4$ ), the value of  $\mu_{\text{mylar}}$  is calculated from its component elements' mass-absorption coefficients:

$$\mu_{\text{mylar}} = \frac{120}{192} \mu_{\text{C}} + \frac{8}{192} \mu_{\text{H}} + \frac{64}{192} \mu_{\text{O}} \quad \text{cm}^2 \text{g}^{-1}, \quad (3.7)$$

where  $\mu_{\text{C}}$ ,  $\mu_{\text{H}}$  and  $\mu_{\text{O}}$  are mass-absorption coefficients for carbon, hydrogen and oxygen respectively.

The X-ray transmission ratio for an absorption foil is given by

$$\frac{I}{I_0} = e^{-\mu x}, \quad (3.8)$$

where  $I$  and  $I_0$  are the intensities of X-ray after attenuation and the incident X-ray while  $\mu$  is the mass absorption coefficient which is a function of X-ray wavelength,  $\lambda$ , and  $x$  is the mass thickness of an x-ray absorber.

### 3.5 Beam Target X-Ray Detection

When electrons are incident onto a target (in this project, either brass or carbon are used as the target), both continuum (Bremsstrahlung) and line radiations are emitted. The total X-ray yield depends on the target material, the incident electron energy and electron beam current.

A relationship for Bremsstrahlung emission based on electron scattering cross section and the Thomas-Whiddington relationship for electron energy loss in the target has been derived [*H. A. Kramers, 1923*], [*N. A. Dyson, 1959*]. The relation is given by

$$I_v = KZ(E_0 - E_v), \quad (3.9)$$

where  $Z$  is the atomic number of the target material;  $E_0$  is the incident electron beam energy;  $E_v$  is the emitted Bremsstrahlung photon energy;  $I_v$  is the intensity of X-ray per unit frequency and  $K$  is a constant. Due to the absorption of the X-ray photons within the target material, this equation must have an angular dependence. The correction factor which is applied to isotropic target material is given by [*J. A. Small et al, 1987*]

$$f_v = \{[1 + 1.2 \times 10^{-6}(E_0^{1.65} - E_v^{1.65})]\mu_a \sin\phi \operatorname{cosec}\theta\}^2, \quad (3.10)$$

where  $\mu_a$  is the mass absorption coefficient ( $\text{cm}^2\text{g}^{-1}$ ) of the anode target,  $\theta$  is the viewing angle relative to the target surface while  $\phi$  is the electron beam incident angle.

If the beam target X-ray is transmitted through an absorption foil with mass absorption coefficient  $\mu_x$  and mass thickness  $\tau$ , and detected by a detector with sensitivity  $S_v$ , the intensity measured is then given by

$$I_{\text{measured}} = \int \frac{I_v}{f_v} e^{-\mu_x \tau} S_v dv \tag{3.11}$$

If two PIN diodes with two different types of foil are used, the ratio of the two signals can be used to deduce the electron beam energy without knowing the value of K. The ratio should be calculated beforehand for certain range of electron beam energy. The graph of the ratio versus electron beam energy, in keV, can be used to deduce the electron beam energy. Since the beam-target interaction will also emit characteristic line radiations, the two absorption foil should be chosen with a thickness that cut off these line radiations. Alternatively the target material can be chosen in such a way that the wavelength of its characteristic line radiation is longer than the cut-off wavelength of the absorption foil.

### 3.6 Three Channel Diode X-Ray Spectrometer - The DXS System

In this project, three channels Diode X-ray Spectrometer (DXS) can be used to obtain the time history of X-ray emissions as well as to determine the electron beam energy by the intensity ratio technique.



The diodes used in the DXS system are BPX-65 PIN diodes. The three PIN diodes are mounted into three “good-fit” holes on a circular brass plate of 5 cm in diameter and 1 cm in thickness. This brass plate containing the diodes is made vacuum tight and is mounted onto a cylindrical brass casing with three BNC free sockets on top of it. The perspective views of the assembly of this system is shown in Figure 3.7. At the front surface side of the brass plate (which will face the X-ray source), an ‘O’-ring surrounds the three diodes as shown in the figure. The DXS system is mounted at the window W2 of the target chamber (see Figure 2.1).

The sensitivities of the three channels PIN diodes are balanced and normalized by obtaining their signals simultaneously from a single discharge at -60 kV of the beam-target X-ray source, with all of them covered with 24  $\mu\text{m}$  aluminised mylar only. One set of the normalised signals is shown in Figure 3.8.

Two set of absorber combinations are used to investigate the energy distribution of the electron beams. The results will be discussed in section 4.4.

Set 1 :

Channel 1 : 24  $\mu\text{m}$  aluminised mylar.

Channel 2 : 36  $\mu\text{m}$  aluminised mylar.

Channel 3 : 24  $\mu\text{m}$  aluminised mylar + 10  $\mu\text{m}$  copper foil.

Set 2 :

Channel 1 : 12  $\mu\text{m}$  aluminised mylar.

Channel 2 : 24  $\mu\text{m}$  aluminised mylar.

Channel 3 : 12  $\mu\text{m}$  aluminised mylar + 10  $\mu\text{m}$  copper foil.

The filtered sensitivity for the two sets of filters are shown in Figure 3.9 and Figure 3.10.

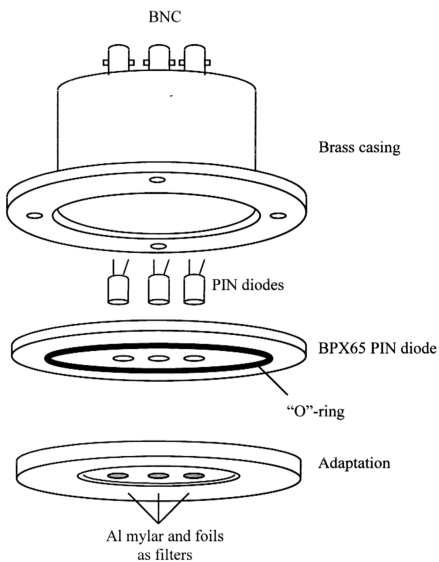


Figure 3.7 The perspective views of the DXS system.

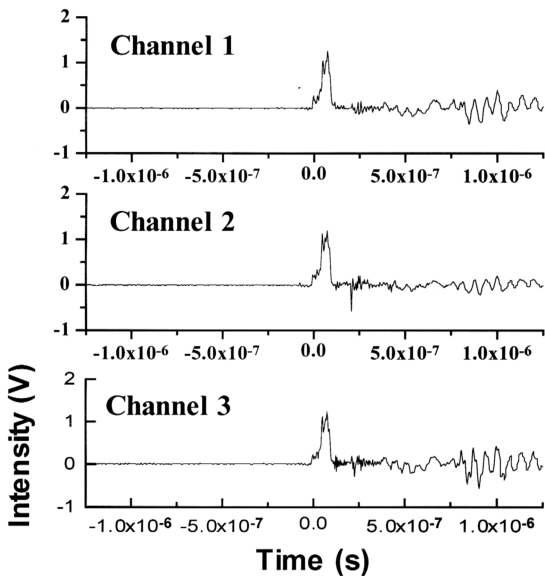


Figure 3.8 Normalised signals of the 3 channels diodes covered with  $24 \mu\text{m}$  aluminised mylar only. The shot is taken at  $1.5 \times 10^{-2}$  mbar for a discharge at  $-60$  kV (#9809034).

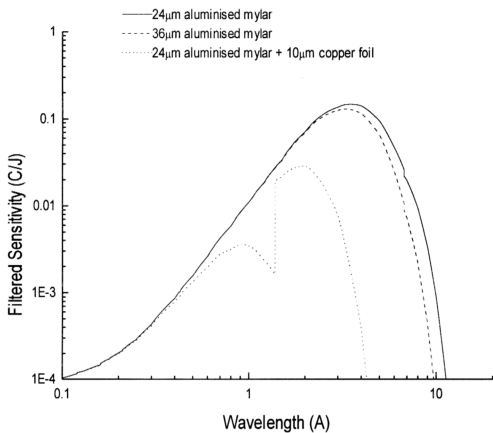


Figure 3.9 The graphs show the filtered sensitivity of BPX65 covered with 24 $\mu$ m; 36 $\mu$ m aluminised mylar and 24 $\mu$ m aluminised mylar + 10 $\mu$ m copper foil.

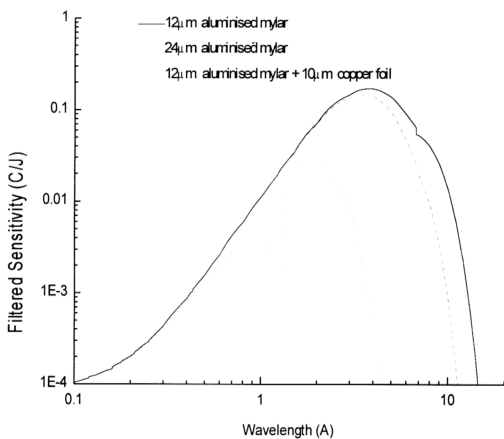


Figure 3.10 The graphs show the filtered sensitivity of BPX65 covered with 12 $\mu$ m; 24 $\mu$ m aluminised mylar and 12 $\mu$ m aluminised mylar + 10 $\mu$ m copper foil.